J Mater Sci: Mater Electron (2017) 28:8588–8595
DOI 10.1007/s10854-017-6582-6

Evaluation of supercapacitive behavior of samarium tungstate nanoparticles synthesized via sonochemical method

Ali Sobhani-Nasab[1] · Hamid Naderi[2] · Mehdi Rahimi-Nasrabadi[3,4] · Mohammad Reza Ganjali[2]

Received: 4 December 2016 / Accepted: 14 February 2017 / Published online: 28 March 2017

Abstract The work focuses on the synthesis of $Sm_2(WO_4)_3$ nanoparticles through a reagent-free aqueous-phase sonochemical reaction between samarium nitrate hexahydrate and $Na_2WO_4.2H_2O$ solutions. The prepared $Sm_2(WO_4)_3$ nano-structures were also characterized by XRD, EDS and SEM to evaluate their structures and morphology. The magnetic properties of as-prepared $Sm_2(WO_4)_3$ nanoparticles were also investigated with vibrating sample magnetometer (VSM). Cyclic voltammetry (CV), galvanostatic charge/discharge and electrochemical impedance spectroscopy (EIS) have been used to investigate the supercapacitive property of the samarium(III) tungstate electrode. The samarium(III) tungstate electrode shows high specific capacitance of 326 F g^{-1} at scan rate of 2 mV s^{-1} in 2.0 M H_2SO_4 electrolyte. Thus, the prepared electrode could be potential electrode materials for supercapacitors.

1 Introduction

Micro- and nano-crystals of metal compounds are subject to considerable attention, due to the specific chemical, electronic, magnetic, and optical properties they present [1–10]. As an instance various rare-earth metal tungstates and molybdates have been found to enjoy excellent properties like good mechanical strength, high oxide ion conductivity properties and excellent thermal and chemical stabilities. Given this ceramics and nano-crystalline tungstates or molybdates of rare-earths have been found useful in display and solid-state laser devices, optical fibers and scintillators [11–13].

Use of novel nano-materials for the purpose of energy efficiency is an important area which can lead to the reduction of fossil fuel consumption and saving the environment [14–19]. Various nano-materials have been suggested for use in energy storage devices such as electrochemical capacitors (ECs). The application of these compounds has been reported to lead to advantages arising from their versatile surface area, morphology and electrochemical properties, which gravely affect the surface and/or interfacial interaction/extraction reactions, which are translated into the improved activity and stability of the devices [20–22].

Electrochemical capacitors (ECs), can be defined as charge-storage devices with very rapid charge and discharge phenomena, offering a unique set of high power and energy, as well as long lifetime. These supercapacitors have recently been treated as energy storage devices with high power densities, long-term cycling stabilities and fast charge/discharge. The outstanding properties of supercapacitors, have changed these devices to promising candidates as energy storage devices in a range of applications like cordless and portable electric equipment's, hybrid and/or electric vehicles, and portable power sources [23–25].

The application of sonochemical reactions for the preparation of materials with novel and unusual properties has proven to be very useful since the 1980s. Ultrasonic irradiations from 20 to 1 MHz have been used as a common

✉ Mehdi Rahimi-Nasrabadi
kpmrahimi@ihu.ac.ir; rahiminasrabadi@gmail.com

1 Young Researchers and Elites Club, Arak Branch, Islamic Azad University, Arak, Iran

2 Center of Excellence in Electrochemistry, University of Tehran, Tehran, Iran

3 Faculty of Pharmacy, Baqiyatallah University of Medical Sciences, Tehran, Iran

4 Department of Chemistry, Imam Hossein University, Tehran, Iran

tool for increasing the rate of various organic, inorganic, and polymerization reactions. The application of ultrasonic irradiation has proven to lead to new chemical reaction mechanisms, further to the acceleration it induces in reaction rates, particularly of those involving heterogeneous systems. These effects can be attributed to the extreme reaction conditions created by the ultrasonic irradiation, which can as an instance provide the high energy levels required for the rearrangement of the structural units of materials in the course of the synthesis process, leading to the formation of new forms of materials [26–30]. In this work, we report synthesis of $Sm_2(WO_4)_3$ nanoparticles via a simple chemical method using $Sm(NO_3)_3{\cdot}6H_2O$ and $Na_2WO_4.2H_2O$ as the starting materials. The sonochemical method is chosen as facile synthetic process due to its flexibility and simplicity. Finally the supercapacitive property of the $Sm_2(WO_4)_3$ electrode were investigated using appropriate techniques.

2 Experimental

2.1 Characterization

The chemicals used were all of analytical grade and none of the chemicals was further treated before use. A Sonicator 3000; Bandeline, MS 72, Germany, Tihorn, 20 kHz, 60 W cm^{-2}, which was directly immersed in the reaction solutions, was used as the source of ultrasonic irradiation. The X-ray diffraction (XRD) patterns were obtained on a Philips-X'PertPro, diffractometer equipped with a Ni-filtered Cu Kα radiation. The scans were made in the range of $10 < 2\theta < 80$. The scanning electron microscopy (SEM) images were recorded by a LEO-1455VP with an energy dispersive X-ray spectroscope. An XL30, Philips microscope was used to obtain the energy dispersive spectrometry (EDS) data and the magnetic measurements on the samples were performed on a vibrating sample magnetometer (VSM), (Meghnatis Daghigh Kavir Co.; Kashan Kavir; Iran) under ambient temperature in magnetic field altering between ±10,000 Oe.

2.2 Synthesis of $Sm_2(WO_4)_3$ nanoparticles

The typical synthesis reaction involved individually dissolving 2 mmol of sodium tungstate dihydrate and 3 mmol of samarium nitrate hexahydrate in two vessels containing 30 mL of distilled water each. The solution containing $Sm(NO_3)_3{\cdot}6H_2O$ was heated to 45 °C for 15 min, before the $Na_2WO_4.2H_2O$ solution was drop-wise added there to and finally the mixture was subjected to a 50 W ultrasonic irradiation. The resulting white product was next separated through filtration, and then rinsed with distilled water and ethanol several times, before a drying step at 60 °C and, followed by calcination at 700 °C for 3 h.

2.3 Electrochemical study

A three-electrode computer controlled Autolab PGSTAT302N workstation was used for the electrochemical evaluations of the behavior of working electrodes prepared through mixing the prepared active materials, carbon black, graphite and PTFE at a mass ratio of 65:20:10:5. To prepare the electrodes, mixtures of the above mentioned ingredients were added to small amounts of absolute ethanol and homogenized to form a slurry. The slurry was used to coat a 1-cm^2 stainless steel element (current collector), and subjected to a pressure of 10 MPa, yielding tablet electrode pads, which were in a final step, dried at 80 °C for 4 h under vacuum. The final electrodes had a mass loading of 3 mg of the active materials. Graphite improves the conductivity of the overall system, covering the high resistance of $Sm_2(WO_4)_3$. Moreover, due to its platelet structure and lubricating properties, it may help the prepared films to be more stable mechanically [21]. The main role of acetylene black is to increase the mass transport through the film, adding additional mesopores. However, it results in better electronic conductivity of the film as well.

The electrochemical evaluations were performed in 2.0 M H_2SO_4 aqueous solutions, and the counter and reference electrodes were a Pt foil and an Ag/AgCl electrode, respectively. Cyclic and continues cyclic voltammetry (CV and CCV); galvanostatic charge/discharge, and electrochemical impedance spectroscopy (EIS) tests were performed to evaluate the electrochemical behavior of the samples. The EIS tests were performed in the range of 100 mHz to 100 kHz under the open circuit potentials (OCPs), at an applied potential of 10 mV. The specific capacitance (SC) values of the electrodes were also evaluated based on cyclic voltammetric data, using the following equation:

$$SC = \frac{\mathrm{i}}{m\nu} = \frac{\int_{V_1}^{V_2} i(V)\, dV}{m\nu\Delta V} \tag{1}$$

in which dV indicates the voltage difference, ν is the scan rate (V s^{-1}), V_1 and V_2 are the initial and final voltage values and m is the mass of the electrode material.

Further the SC values can be calculated based on the charge/discharge data using the following equation:

$$SC = \frac{I\Delta t}{\Delta V} \tag{2}$$

where I and Δt represent the charge/discharge current (A) and discharge time (s); and V is the potential drop during discharge (V).

3 Results and discussion

To study the crystalline structure and composition of the sample, they were studied by XRD and a sample results is illustrated in Fig. 1. The XRD pattern in this figure and the diffraction peaks in it fully complied with the pure monoclinic phase of $Sm_2(WO_4)_3$ with C2/c space groups and JCPDS No. 23-0525. Since no unidentified diffraction peaks were observed the sample was considered to be pure. The XRD data also proved the crystallite diameter (Dc) of $Sm_2(WO_4)_3$ the particles to be 18 nm, based on the Scherer equation:

$$D_c = K\lambda/\beta \cos\theta$$

In which β represents the breadth of the diffraction line at its half intensity maximum (400), K is the shape factor (usually about 0.9), and λ shows the wavelength of X-ray source. Further morphology studies using SEM (Fig. 2), revealed the presence of uniform spherical nanoparticles with average particle sizes in the range of 50–55 nm. The results of EDS analyses (Fig. 3) also proved the purity of the sample. The VSM magnetic measurements on the nanoparticles calcinated at 700 °C (Fig. 4) showed the $Sm_2(WO_4)_3$ nanoparticles to have a paramagnetic behavior and a saturation magnetization of 0.017 emu g^{-1} at the ambient temperature.

3.1 CV, specific capacitances and CCV

It is well-known that CV can provide a set of important information on the super-capacitive behaviors of electrodes. The CV curves obtained for $Sm_2(WO_4)_3$ based electrodes are given in Fig. 5a. These voltammograms were obtained in the optimized potential range of −0.4–0.35 V (vs. Ag/AgCl) under different scan rates (5–100 mV s^{-1}). Figure 5b illustrates the SC behavior as a function of the scan rates. It is clear that the SCs of the $Sm_2(WO_4)_3$-electrode drops from 326 to 197 F g^{-1} upon changing the scan rate from 2 to 200 mV s^{-1}. This can be attributed to the fact that lower scan rates provide the electrolyte ions (i.e., H^+) with ample time to diffuse into the pores of the electrode material, which provides higher surfaces for the effective redox reactions. On the other hand, at higher scan rates these ions have only a limited time window in which they can only access the outer surface of the material, hence lowering the total SC.

The measured capacitance is mainly governed by faradaic redox mechanism, and the reaction is based on the reversible redox of Sm^{2+} to Sm^{+3} [31].

$$Sm^{3+} + e^- Sm^{2+}$$

Here the pseudocapacitance behavior comes mainly from the faradic redox reaction of Sm and the role of W is to enhance the electrical conductivity of the $SmWO_4$

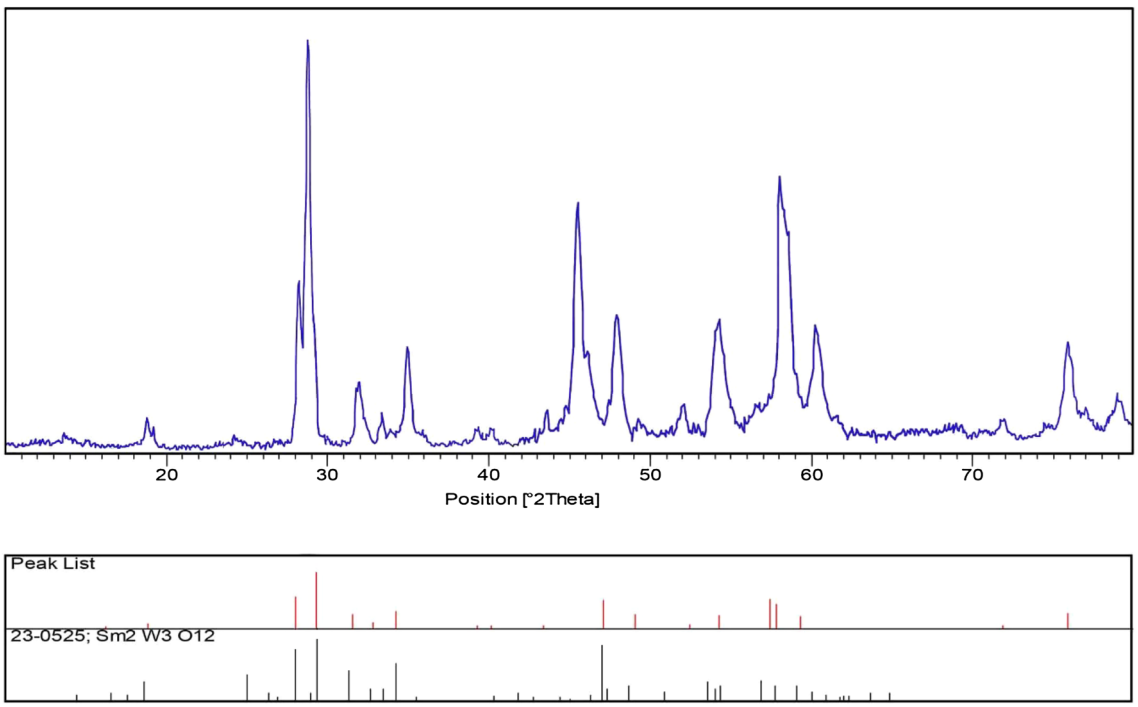

Fig. 1 XRD pattern of $Sm_2(WO_4)_3$ nanoparticles

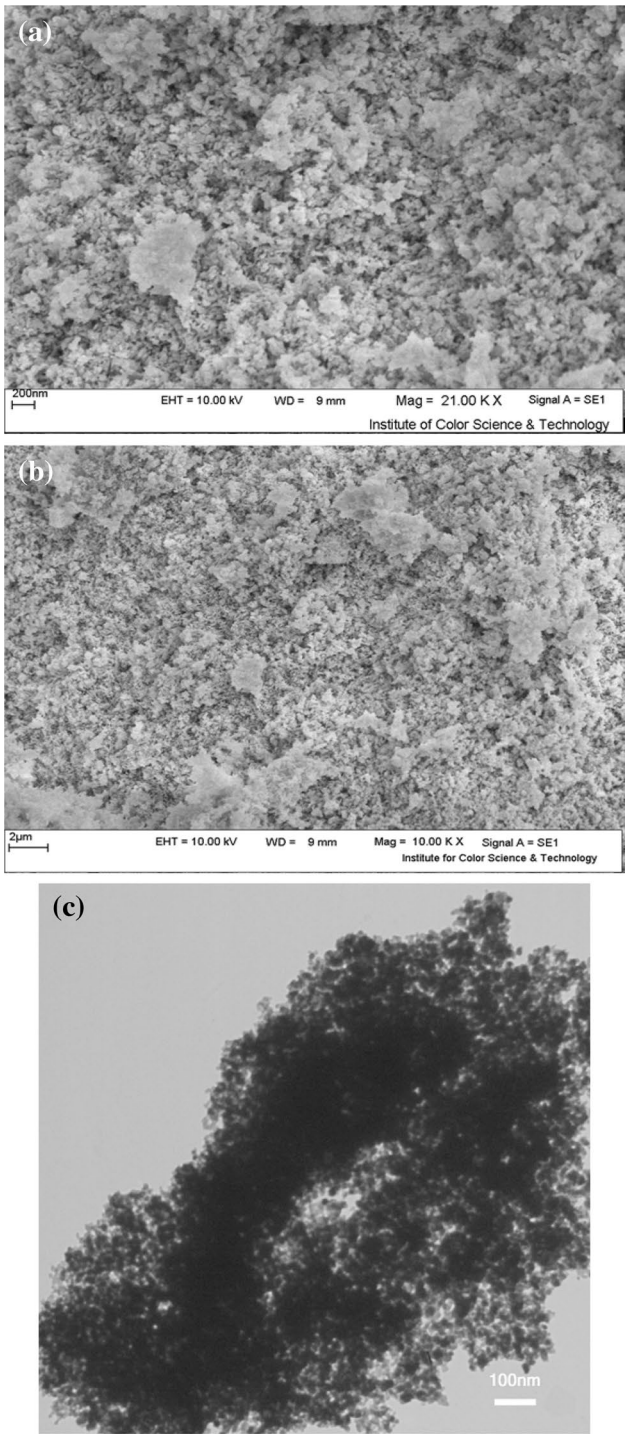

Fig. 2 **a, b** SEM images of $Sm_2(WO_4)_3$ nanoparticles, **c** TEM images of $Sm_2(WO_4)_3$ nanoparticles

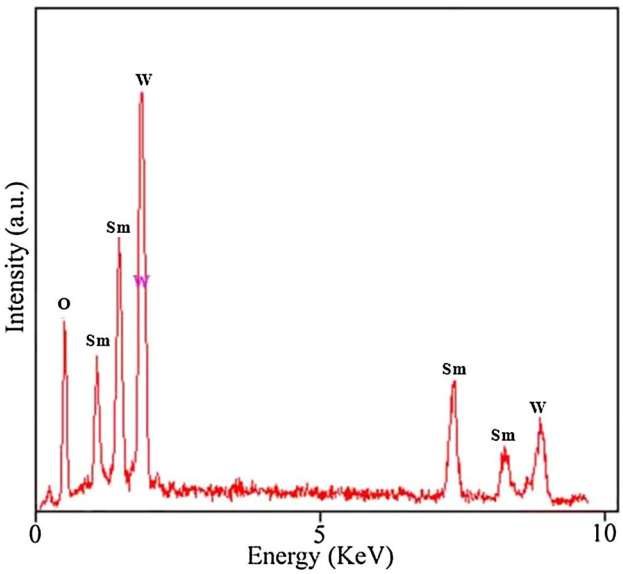

Fig. 3 EDS pattern of $Sm_2(WO_4)_3$ nanoparticles

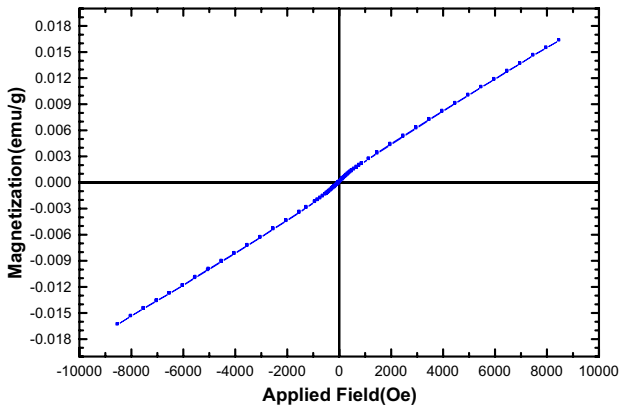

Fig. 4 VSM curve of $Sm_2(WO_4)_3$ nanoparticles

materials [32]. The redox behavior of W has no contribution to the measured capacitance.

Continues cyclic voltammetry (CCV) can be seen as the best tool for examining the changes in the charge storage of a capacitor during potential cycling [33–35]. In the course of CCV the stability of the electrodes is assessed under long-term potential cycles. Three-dimensional CCVs of the $Sm_2(WO_4)_3$ electrode obtained at 200 mV s^{-1} in a 2.0 M H_2SO_4 solution are illustrated in Fig. 5c The 3D-plot indicates the changes in the CVs over the number of cycles to be rather noticeable. Further the calculated SC values for each CV, as a function of the number of cycles are shown in Fig. 5d. As shown in Fig. 5d, the SC of $Sm_2(WO_4)_3$ electrode retain at 89.9% of its original value, at scan rate 200 mV s^{-1} for 4000 cycles. This high stability suggests that the $Sm_2(WO_4)_3$ electrodes can be regarded as suitable for application in fast charging devices.

According to the results of CV and CCV, supercapacitive performance of $Sm_2(WO_4)_3$ electrode is much better compared to other works that are presented in Table 1. As

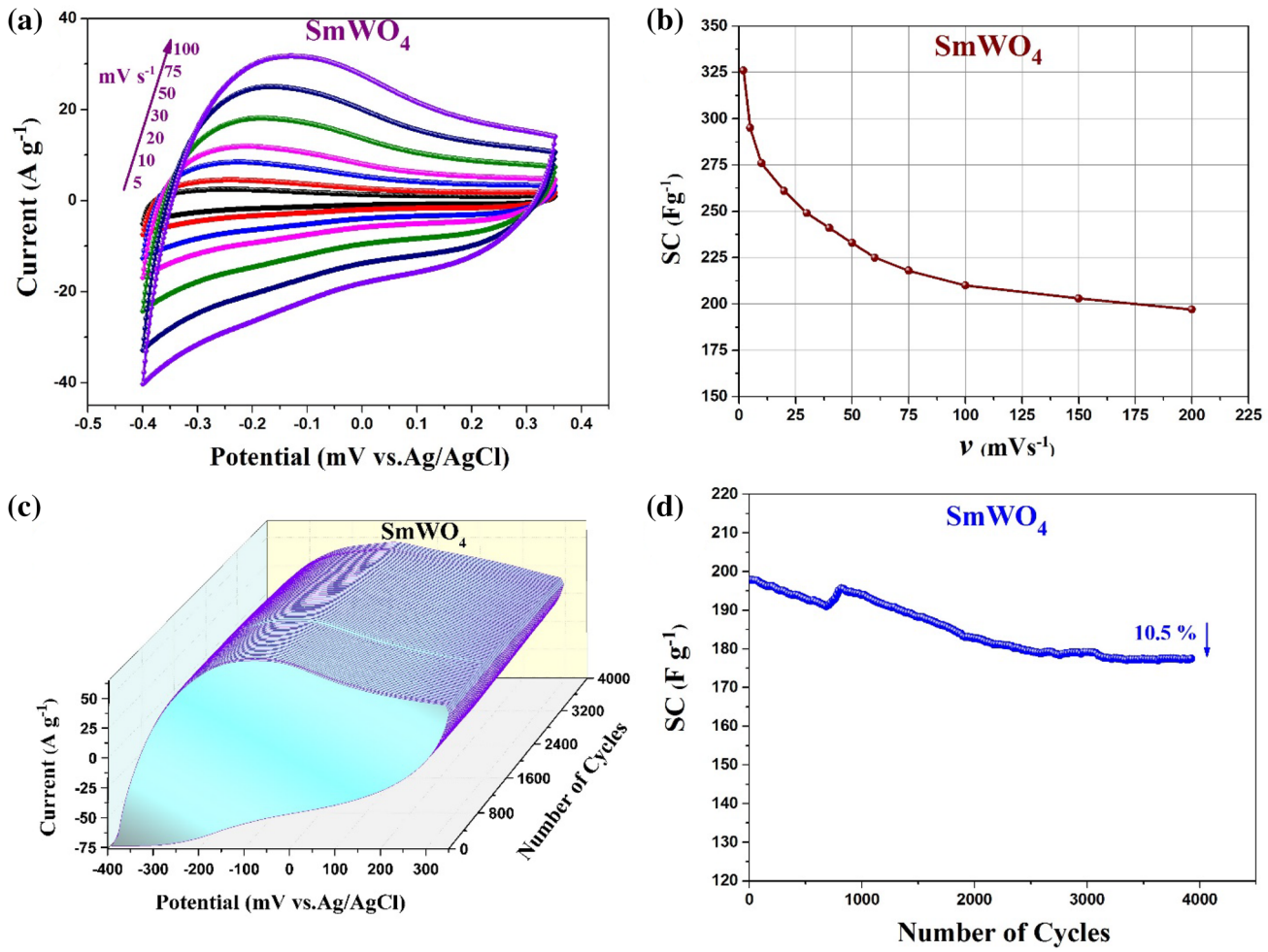

Fig. 5 **a** CVs of the $Sm_2(WO_4)_3$ electrode at different scan rates of 5, 10, 20, 30, 50, 75 and 100 mV s^{-1} in a potential range of −0.4–0.35 Vin 2.0 M H_2SO_4 aqueous electrolyte, **b** specific capacitance as a function of the sweep rates for the $Sm_2(WO_4)_3$ electrode, **c** 3D-CCV curves of the $Sm_2(WO_4)_3$ electrode measured at scan 200 mV $s^{-1}$and **d** variation of the specific capacitance of the $Sm_2(WO_4)_3$ electrode as a function of number of cycles at 200 mV s^{-1}

Table 1 Comparison of supercapacitive behavior of between $Sm_2(WO_4)_3$ electrode and some reported metal tungstate nanostructure electrodes

	Electrolyte	Potential window (V)	Specific capacitance	Cycling stability	Ref.
$SnWO_4$	3.0 M KOH	0.0–0.55	242 F g^{-1} (5 mV s^{-1})	85% (4000 cycles)	[31]
ZnWO4	2.0 M KOH	0.0–0.6	35.7 F g^{-1} (0.25 A g^{-1})	–	[36]
$FeWO_4$	5 M $LiNO_3$	−0.6–0.0	35 F g^{-1} (10 mV s^{-1})	93.0% (10,000 cycles)	[37]
$MnWO_4$	0.1 M Na_2SO_4	0.0–1.0	34 F g^{-1} (0.5 mA cm^{-2})	–	[38]
$NiWO_4$	2.0 M KOH	0.0–0.6	173 F g^{-1} (5 mV s^{-1})	90% (1000 cycles)	[39]
$CuWO_4$	0.5 M HCl	−0.1–0.8	77 F g^{-1} (5 mV s^{-1})	–	[40]
$CoWO_4$	2.0 M KOH	−0.25–0.45	60.6 F g^{-1} (5 mV s^{-1})	94.7% (1000 cycles)	[41]
$SmWO_4$	2.0 M H_2SO_4	−0.8–0.2	321 F g^{-1} (2 mV s^{-1})	99.0% (4000 cycles)	This work

can be seen in Table 1, the maximum SC and stability of $Sm_2(WO_4)_3$ electrode are higher than SC and stability of metal tungstate nanostructure electrodes that have been investigated in aqueous electrolytes so far [31, 36–41].

3.2 Galvanostatic charge/discharge

Galvanostatic charge/discharge analyses constitute a dependable means for assessing the super-capacitive

performance of materials under controlled conditions. The tests were performed in a two-electrode system and in a potential window of −0.4–0.35 V (vs. Ag/AgCl), and the results are illustrated in Fig. 6a. The figure contains the charge/discharge curves of the $Sm_2(WO_4)_3$ electrodes at various current densities of 1–16 A g^{-1}. It is evident that all curves have equilateral triangular shapes, indicating acceptable reversibility and ideal capacitive behaviors.

The plot of the SC versus current density behavior is illustrated in Fig. 6b. The decrease of maximum 44.7% in the SC even at current densities as high as 32 A g^{-1}, which can be observed in this figure, is an indication of the outstanding capacitive retaining tendency of the electrode material and the SC values obtained are in good agreement with the CV data.

To evaluate the power performance of the $Sm_2(WO_4)_3$ electrodes, the Ragone (power density versus energy density) plots were used. Figure 7, shows the energy and

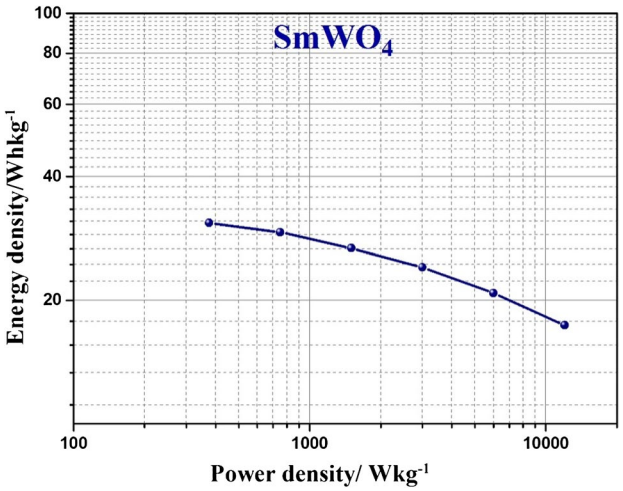

Fig. 7 Ragone plots obtained for the $Sm_2(WO_4)_3$ electrode

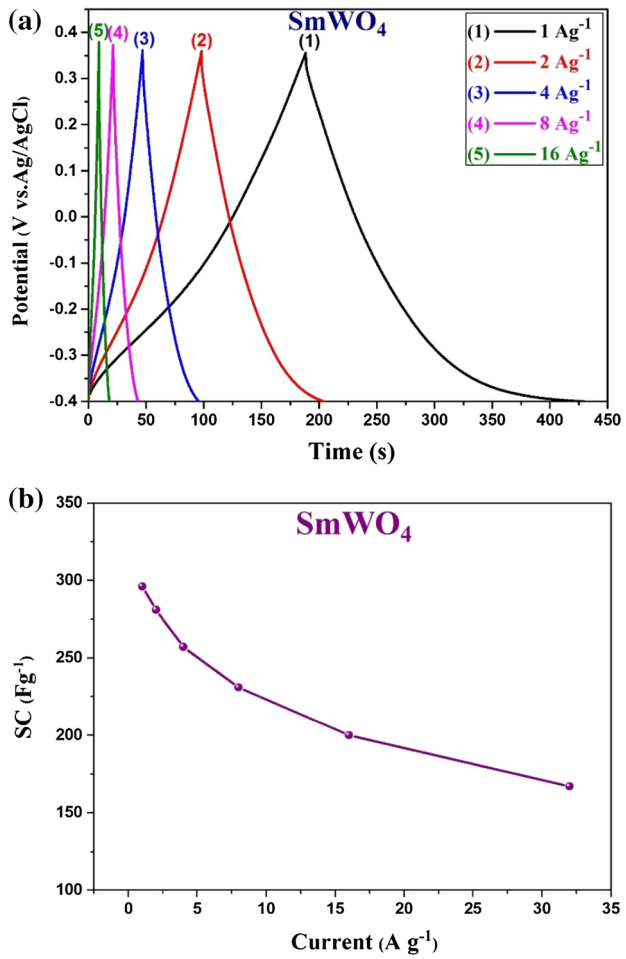

Fig. 6 **a** Charge/discharge curves of the $Sm_2(WO_4)_3$ electrode at different charge/discharge current densities between −0.4 and 0.35 V in 2.0 M H_2SO_4 aqueous electrolyte, **b** variation of SC at different current density for the $Sm_2(WO_4)_3$ electrode

power densities obtained from charge/discharge analyses at different current densities. The maximum energy density value for the $Sm_2(WO_4)_3$ electrode was found to be 30.8 W h Kg^{-1} (at a power density of 350 W Kg^{-1}), which is much higher than those of similar electrodes in aqueous electrolyte media [42, 43]. This helped decide that the $Sm_2(WO_4)_3$ electrodes can be used suitable for use in supercapacitors.

3.3 Electrochemical impedance spectroscopy (EIS)

Electrochemical impedance spectroscopy is a prominent technique for studying the supercapacitive and typical resistance of electrode materials. The Nyquist plots presented obtained for the $Sm_2(WO_4)_3$ electrodes in the range of 0.1–105 Hz under open circuit potentials, are presented in Fig. 7. The EIS spectra include combinations of a semicircle, in high frequencies, and a straight line for low frequencies. The equivalent circuit for the Nyquist plots shown as an inset in Fig. 7, uses the R_s, R_{ct}, C_{dl}, $Z_{w,}$ and C_F symbols to refer to solution and charge-transfer resistance values, double layer capacitance, and Warburg impedance, respectively [44]. R_s was calculated to be 1.66 Ω for the $Sm_2(WO_4)_3$ electrodes and the inset in the Fig. 8 illustrates the expanded high frequency region of impedance. R_{ct} is an electrode/electrolyte interfacial charge transfer resistance, and is 10.20Ω as indicated by the diameter of the semicircle. The low R_{ct} values obtained for the $Sm_2(WO_4)_3$ electrodes indicated the electrochemical reaction at the electrode/electrolyte interface to be more facile in the case of the proposed electrode material. C_{dl} represents the capacitance of the electrical double layer at the electrode/electrolyte interface and C_F illustrates the pseudo-capacitance of the faradic

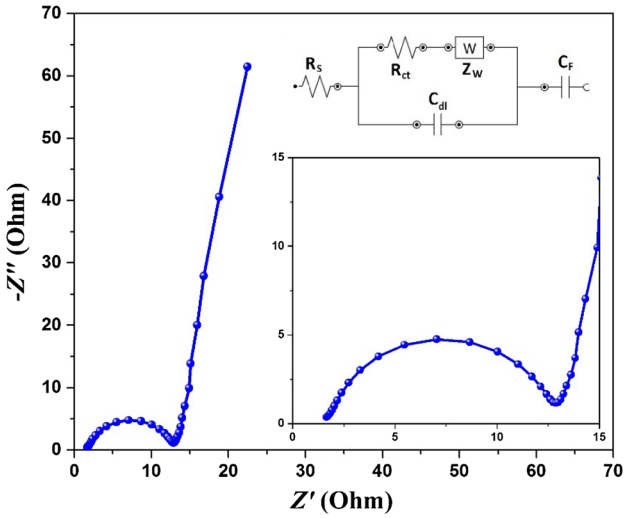

Fig. 8 Impedance spectra of the $Sm_2(WO_4)_3$ electrode, measured at an AC amplitude of 10 mV, in 2.0 M H_2SO_4 aqueous electrolyte

reaction. C_{dl} and C_F of the $Sm_2(WO_4)_3$ electrodes were found to be 0.241 and 322 mF, respectively. Further Z_W is (i.e., Warburg resistance) which shows the frequency behavior of the ion diffusion/transport toward the electrode surface [45]. The studies indicated the $Sm_2(WO_4)_3$ electrodes to show near-to-ideal Warburg resistance; where a more vertical line indicates that the electrode is closer to an ideal capacitor. This proved to be also consistent with the data obtained from CVs and charge/discharge experiments.

4 Conclusion

$Sm_2(WO_4)_3$ nanoparticles were synthesized through a reagent-free sonochemical method in aqueous media and the EDS and XRD studies confirmed the high purity of the sample. Further evaluations by SEM, UV–Vis, and VSM techniques were made to characterize the nano-structured product. The $Sm_2(WO_4)_3$ electrode shows high specific capacitance of 326 F g^{-1} at scan rate of 2 mV s^{-1}. Moreover, an excellent rate performance was also observed during the continuous 4000 cycles. $Sm_2(WO_4)_3$ electrode shows good stability in CCV test and after 4000 cycles the SC of electrode retain at 89.9% of its original value, at scan rate 200 mV s^{-1}. This high stability suggests that the prepared electrode could be potential electrode materials for supercapacitors.

Funding The authors are gratefully acknowledged the financial support provided by Iran National Science Foundation (Project 94019559).

References

1. F. Ahmadi, M. Rahimi-Nasrabadi, A. Fosooni, M.H. Daneshmand, J. Mater. Sci. Mater. Electron. doi. 10.1007/s10854-016-5002-7 (2016)
2. M. Rahimi-Nasarabadi, F. Ahmadi, S. Hamdi, N. Eslami, K. Didehban, M.R. Ganjali, J. Mol. Liq. **216**, 814 (2016)
3. Y. Fazli, S.M. Pourmortazavi, I. Kohsari, M.S. Karimi, M. Tajdari, J. Mater. Sci. Mater. Electron. **27**, 7192 (2016)
4. M. Rahimi-Nasrabadi, M. Behpour, A. Sobhani-Nasab, S. M. Hosseinpour-Mashkani, J. Mater. Sci. Mater. Electron. **26**, 9776 (2015)
5. S.M. Pourmortazavi, M. Rahimi-Nasrabadi, Y. Fazli, M. Mohammad-Zadeh, Int. J. Refract. Met. Hard Mater. **51**, 29 (2015)
6. S.M. Pourmortazavi, M. Taghdiri, N. Samimi, M. Rahimi-Nasrabadi, Mater. Lett. **121**, 5 (2014)
7. M. Shamsipur, S.M. Pourmortazavi, M. Roushani, S.S. Hajimirsadeghi. Synth. React. Inorg. Met.-Org. Chem. **44**, 951 (2014)
8. S.M. Pourmortazavi, A. Zaree, S. Mirsadeghi, J. Sol-Gel Sci. Technol. **76**, 510 (2015)
9. M. Ramezani, S. M. Pourmortazavi, M. Sadeghpur, A. Yazdani, I. Kohsari, J. Mater. Sci. Mater. Electron. **26**, 3861 (2015)
10. S.M. Pourmortazavi, Z. Marashianpour, M. Sadeghpour Karimi, M. Mohammad-Zadeh, J. Mol. Struct. **1099**, 232 (2015)
11. M. Rahimi-Nasrabadi, S.M. Pourmortazavi, M.R. Ganjali, A.R. Banan, F. Ahmadi, J. Mol. Struct. **1074**, 85 (2014)
12. S.M. Pourmortazavi, M. Rahimi-Nasrabadi, Y. Fazli, M. Mohammad-Zadeh, Appl. Phys. A **119**, 929 (2015)
13. M. Rahimi-Nasrabadi, S.M. Pourmortazavi, M.R. Ganjali, P. Norouzi, F. Faridbod, M. Sadeghpour Karimi, J. Mater. Sci. Mater. Electron. doi: 10.1007/s10854-016-5421-5 (2016)
14. M. Esmaili, A. Habibi-Yangjeh, J. Iran. Chem. Soc. **7**, 70 (2010)
15. M. Rahimi-Nasrabadi, F. Ahmadi, A. Fosooni, J. Mater. Sci. Mater. Electron. **28**, 537 (2017)
16. V. Taghvaei, A. Habibi-Yangjeh, M. Behboudnia, J. Iran, Chem. Soc. **7**, 175 (2010)
17. M. Rahimi-Nasrabadi, F. Ahmadi, M. Eghbali-Arani, J. Mater. Sci. Mater. Electron. **27**, 11873 (2016)
18. M. Shekofte-Gohari, A. Habibi-Yangjeh, Ceram. Int. **41**, 1467 (2015)
19. M. Rahimi-Nasrabadi, M. Behpour, A. Sobhani-Nasab, M. Rangraz Jeddy, J. Mater. Sci. Mater. Electron. **27**, 11691 (2016)
20. J. Tizfahm, M. Aghazadeh, M. Ghannadi Maragheh, M.R. Ganjali, P. Norouzi, F. Faridbod, Mater. Lett. **167**, 153 (2016)
21. H.R. Naderi, M.R. Ganjali, P. Norouzi, Int. J. Electrochem. Sci. **11**, 4267 (2016)
22. H.R. Naderi, M.R. Ganjali, A. Shiralizadeh Dezfuli, P. Norouzi, RSC Adv. **6**, 51211 (2016)
23. M. Aghazadeh, M. Ghannadi Maragheh, M.R. Ganjali, P. Norouzi, RSC Adv. **6**, 10442 (2016)
24. J.S. Shayeh, A. Ehsani, M.R. Ganjali, P. Norouzi, B. Jaleh, Appl. Surf. Sci. **353**, 594 (2015)
25. M. Aghazadeh, M. Asadi, M.G. Maragheh, M.R. Ganjali, P. Norouzi, F. Faridbod, Appl. Surf. Sci. **364**, 726 (2016)
26. S.M. Hosseinpour-Mashkani, A. Sobhani-Nasab, J. Mater. Sci. Mater. Electron. **27**, 3240 (2016)
27. H. Nouri, A. Habibi-Yangjeh, Phys. Chem. Res. **3**, 99 (2015)
28. S. Naghizadeh-Alamdari, A. Habibi-Yangjeh, J. Iran. Chem. Soc. **12**, 1961 (2015)
29. M. Shekofteh-Gohari, A. Habibi-Yangjeh, J. Colloid Interface Sci. **461**, 144 (2016)
30. S. Shaker-Agjekandy, A. Habibi-Yangjeh, Mater. Sci. Semicond. Process. **44**, 48 (2016)
31. S.R. Ede, S. Kundu, ACS Sustain. Chem. Eng. **3**, 2321 (2015)

32. L. Niu, Z. Li, Y. Xu, J. Sun, W. Hong, X. Liu, J. Wang, S. Yang. ACS Appl. Mater. Interfaces **5**, 8044 (2013)
33. H.R. Naderi, H.R. Mortaheb, A. Zolfaghari, J. Electroanal. Chem. **719**, 98 (2014)
34. H.R. Naderi, P. Norouzi, M.R. Ganjali, Mater. Chem. Phys. **163**, 38 (2015)
35. A.S. Dezfuli, M.R. Ganjali, H.R. Naderi, P. Norouzi, RSC Adv. **5**, 46050 (2015)
36. R.D. Kumara, Y. Andoub, S. Karuppuchamy, J. Phys. Chem. Solids **92**, 94 (2016)
37. N. Goubard-Bretesché, O. Crosnier, C. Payen, F. Favier, T. Brousse. Electrochem. Commun. **57**, 61 (2015)
38. U. Nithiyanantham, S.R. Ede, T. Kesavan, P. Ragupathy, M.D. Mukadam, S.M. Yusuf, S. Kundu, RSC Adv. **4**, 38169 (2014)
39. S.R. Ede, S. Anantharaj, S. Kundu, Cryst. Growth Des. **15**, 673 (2015)
40. R.D. Kumar, S. Karuppuchamy, Ceram. Int. **40**, 12397 (2014)
41. X. Xu, J. Shen, N. Li, M. Ye, Electrochim. Acta **150**, 23 (2013)
42. H.R. Naderi, P. Norouzi, M.R. Ganjali, Appl. Surf. Sci. **366**, 552 (2016)
43. K. Adib, M. Rahimi-Nasrabadi, Z. Rezvani, S.M. Pourmortazavi, F. Ahmadi, H.R. Naderi, M.R. Ganjali, J. Mater. Sci. Mater. Electron. **27**, 4541 (2016)
44. S.R. Ede, A. Ramadoss, U. Nithiyanantham, S. Anantharaj, S. Kundu, Inorg. Chem. **54**, 3851 (2015)
45. A. Zolfaghari, H.R. Naderi, H.R. Mortaheb, J. Electroanal. Chem. **697**, 60 (2013)